Mobile Metal-Metal Bonds: Studies on Mixed Valence Ir_3 and Ir_4 Clusters

Anne Venturelli and Thomas B. Rauchfuss*

Contribution from the School of Chemical Sciences, University of Illinois, Urbana, Illinois 61801

Received January 7, 1994®

Abstract: The dicationic clusters $[(C_5Me_5)_4Ir_4S_4]^{2+}$ ($[1]^{2+}$) and $[(C_5Me_5)_3Ir_3S_2]^{2+}$ ($[2]^{2+}$) were prepared by treatment of $[(C_5Me_5)IrCl_2]_2$ with $(Me_3Si)_2S$ followed by ion exchange chromatography. Crystallographic characterization of the tetrairidium cluster $[1]^{2+}$ reveals a cubane motif consisting of interpenetrated Ir_4 and S_4 tetrahedra. The Ir_4 core is distorted from idealized tetrahedral symmetry by virtue of a single Ir^{IV}-Ir^{IV} bonding contact of 2.764(1) Å. The four Ir^{IV}-Ir^{III} contacts are nearly equivalent at 3.5 Å, while the $Ir^{III}\cdots Ir^{III}$ distance is 3.683(1) Å. Variable-temperature ^1H NMR studies indicate that $[1]^{2+}$ is fluxional with a coalescence temperature of 13 °C (400 MHz), corresponding to $\Delta G^{\ddagger}$ = 57 kJ/mol. This dynamic process is attributed to migration of the metal-metal bond arising from internal Ir^{IV}/Ir^{III} self-exchange. Cyclic voltammetry studies of $[1]^{2+}$ reveal a pair of reversible one-electron reductions at -218 and -487 mV vs Ag/AgCl. Chemical reduction of $[1]^{2+}$ was effected with cobaltocene while the neutral cluster could be reoxidized with HCl/O_2. In the solid state $[2]^{2+}$ features a trigonal-bipyramidal Ir_3S_2 core with average Ir-Ir contacts of 2.82 Å and Ir-S distances of 2.28 Å. Cyclic voltammetry studies indicate that this closo dication undergoes two single electron reductions at -712 and -993 mV. Cobaltocene reduction of $[2]^{2+}$ afforded dark blue crystals of neutral $[2]^0$. Variable-temperature ^1H NMR spectra of $[2]^0$ reveal dynamic behavior, with coalescence at 60 °C (400 MHz), corresponding to $\Delta G^{\ddagger}$ = 64 kJ/mol. These structural dynamics suggest migration of the nonbonding Ir···Ir interaction among the three edges of the Ir_3 triangle.

Introduction

The dynamics of chemical bonds represent a particularly fundamental process. Cases where these dynamics are degenerate and intramolecular are particularly instructive. A molecule which illustrates this phenomenon is bullvalene where all ten carbon centers equilibrate readily at room temperature, eq 1.[1] Cor-

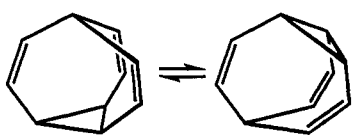

(1)

responding examples of skeletal rearrangements involving metal-metal bonds were not known when we began this work. Of course many compounds, metal-containing and otherwise, exhibit dynamic structures (fluxionality), but these dynamics are almost always coupled to or driven by changes in ligation or electron count.[2,3] Our interests focus on the mobility of metal-metal bonds in the absence of other changes in the coordination environment about the metals. The degenerate bond/no-bond interchange within a cluster framework is the specific phenomenon of interest.

The cubane clusters $(C_5R_5)_4M_4(\mu_3\text{-}E)_4$ are especially appealing subjects for the study of the dynamics of metal-metal bonds. Clusters of this category have been prepared for many metals and many main group vertices (E).[4] Furthermore, many of these species exist in multiple oxidation states. Important for our studies is the fact that this series of clusters displays systematic structural changes which correlate to cluster electron count. Specifically,

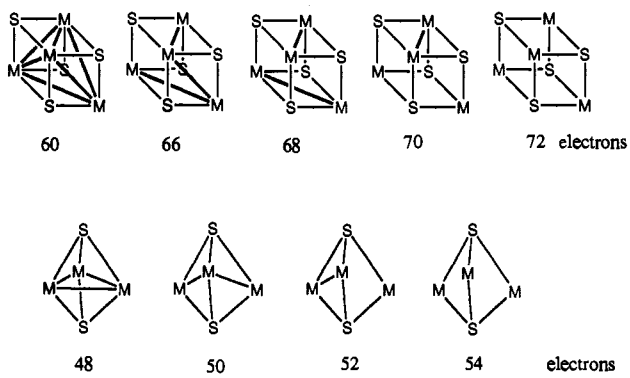

Figure 1. Idealized structures of $(C_5R_5)_4M_4E_4$ and $(C_5R_5)_3M_3E_2$ cluster cores showing patterns of localized M-M bonding as a function of electron count.

the number of metal-metal bonds in the $(C_5R_5)_4M_4(\mu_3\text{-}E)_4$ clusters corresponds well, but not perfectly,[5] with cluster electron count. In general, the intermetallic distances increase as the cluster electron count increases from 60 to 72. The fact that this trend is the reverse of that seen for metal radii is strong evidence for the dominant role of metal-metal interactions. For the sulfido cubane clusters the electron counts represent the sum of 24 e^- from the four S^{2-} vertices and 36 e^- from the four $C_5R_5^-$ ligands, in addition to the valence d electrons associated with the four trivalent metals. The net metal-metal bond order for the members of this series ranges from six for the 60 e^- Mo_4 clusters to zero for 72 e^- Co_4 species,[6] see Figure 1. This trend indicates that the acceptor orbitals in these >60 e^- clusters are metal-metal antibonding. Clusters with electron counts intermediate between 60 and 72 are expected to exhibit net metal-metal bond

® Abstract published in *Advance ACS Abstracts,* May 1, 1994.

(1) (a) Doering, W. von E.; Roth. W. R. *Angew. Chem., Int. Ed. Engl.* **1963**, *2*, 115; *Angew. Chem.* **1963**, *75*, 27. (b) Schröder, G. *Angew. Chem., Int. Ed. Engl.* **1963**, *2*, 481; *Angew. Chem.* **1963**, *75*, 722.

(2) For examples see: (a) Edidin, R. T.; Zyzyck, L. A.; Norton, J. R. *J. Chem. Soc., Chem. Commun.* **1979**, 580. (b) Kubas, G.; Vergamini, P. J. *Inorg. Chem.* **1981**, *20*, 2667. (c) Bailey, D. A.; Balch, A. L.; Fossett, L. A.; Olmstead, M. M.; Reedy,d P. E., Jr. *Inorg. Chem.* **1987**, *26*, 2413.

(3) The exception to this pattern is the dynamic interchange of long and short W-W bonding interactions in $W_4(O\text{-}i\text{-}Pr)_{12}$. Chisholm, M. H.; Clark, D. L.; Hampden-Smith, M. J. *J. Am. Chem. Soc.* **1989**, *111*, 574.

(4) Harris, S. *Polyhedron* **1988**, *8*, 2843.

(5) $(C_5H_5)_4Cr_4O_4$ is antiferromagnetic: (a) Bottomley, F.; Paez, D. E.; Sutin, L.; White, P. S.; Köhler, F. H.; Thompson, R. C.; Westwood, N. P. C. *Organometallics* **1990**, *9*, 2443. (b) Bottomley, F.; Chen, J.; MacIntosh, S. M.; Thompson, R. C. *Organometallics* **1991**, *10*, 906.

(6) (a) Williams, P. D.; Curtis, M. D. *Inorg. Chem.* **1986**, *25*, 4562. (b) Bandy, J. A.; Davies, C. E.; Green, J. C.; Green, M. L. H.; Prout, K.; Rodgers, D. P. S. *J. Chem. Soc., Chem. Commun.* **1983**, 1395. (c) Simon, G. L.; Dahl, L. F. *J. Am. Chem. Soc.* **1973**, *95*, 2164.

0002-7863/94/1516-4824$04.50/0

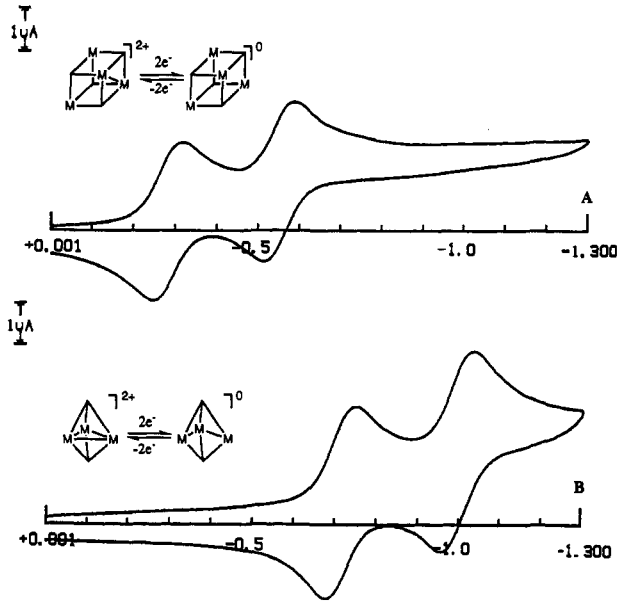

Figure 2. Cyclic voltammograms of CH_2Cl_2 solutions of $[(C_5Me_5)_4Ir_4S_4](PF_6)_2$ (A) and $[(C_5Me_5)_3Ir_3S_2](PF_6)_2$ (B) referenced to Ag/AgCl, with a scan rate of 100 mV/s.

orders intermediate between six and zero. The cluster $(RC_5H_4)_4Fe_4S_4$ follows this pattern with two short (bonding) Fe–Fe contacts of 2.6 Å.[7,8] Similar patterns are seen in other low-spin Fe–S and Fe–Se clusters.[9]

The structures of the $(C_5R_5)_3M_3E_2$ clusters correlate with their electron counts as determined by Wade's rules.[10] Those with 48 e^- typically exhibit three metal–metal bonds while those with 54 e^- are predicted to contain no metal–metal bonds (Figure 1). The energetically subtle distinction between localized and delocalized M–M interactions is illustrated by Otsuka's 50 e^- clusters of the type $(C_5R_5)_3Co_3S_2$, which have been extensively studied by the Dahl group. Such species adopt both D_{3h} and C_{2v} structures depending on the substituents on the cyclopentadienyl ligands.[11] Our experience indicates that such subtleties are less important for clusters derived from the second- and third-row metals. This point is illustrated by the neutral and dicationic clusters of the type $[(cymene)_3Ru_3S_2]^z$, which have been examined by single crystal X-ray diffraction.[12] The oxidized ($z = 2+$) and reduced ($z = 0$) states adopt spin-paired closo (D_{3h}) and nido (C_{2v}) structures, respectively. Similar structural trends have been observed for phosphinidene clusters of the type $Fe_3(PR)_2(CO)_9$.[13]

Our interests in mobile metal–metal bonds originated with the finding that the 66 e^- cluster $[(RC_5H_4)_4Ru_4S_4]^{2+}$ adopts a localized structure in the solid state with three Ru–Ru bonding interactions.[14] Solution NMR experiments show that this same structure exists in solution, although at higher temperatures the two different sites equilibrate. We proposed that this equilibration involves the shifting of metal–metal bonds within the cluster. This $Ru^{III}_2Ru^{IV}_2$ system provides the only case of metal–metal bond–no bond equilibria in clusters. Given what we believe to be the fundamental nature of this phenomenon, we have sought other examples of mobile metal–metal bonds. Of particular interest was a cubane cluster featuring one bond. The synthetic method used to achieve this goal provided a M_3 cluster which also exhibits mobile metal–metal bonds.

Results

Synthesis of $[(C_5Me_5)_4Ir_4S_4]^{2+}$ and $[(C_5Me_5)_3Ir_3S_2]^{2+}$. Treatment of a methanol/THF slurry of $[(C_5Me_5)IrCl_2]_2$ with $(Me_3Si)_2S$ produced a mixture of water-soluble products which were separated into green and yellow fractions using ion exchange chromatography. Addition of excess KPF_6 to each fraction precipitated CH_2Cl_2-soluble salts analyzing as $[(C_5Me_5)_3Ir_3S_2](PF_6)_2$ ($[\mathbf{2}]^{2+}$) and $[(C_5Me_5)_4Ir_4S_4](PF_6)_2$ ($[\mathbf{1}]^{2+}$) in 54 and 4% yields, respectively. These formulations were supported by FAB mass spectrometry, elemental analysis, and X-ray crystallography (see below).

The formation of the Ir_3 cluster can be rationalized on the basis of the stoichiometry of the reactants (eq 2). The observation of the mixed valence cluster $[\mathbf{1}]^{2+}$ suggests that the $CH_3OH/(Me_3Si)_2S$ mixture generates a species capable of oxidizing some of the iridium to the tetravalent state. This oxidation is associated with the methanolysis of $(Me_3Si)_2S$, since the reaction of $[(C_5Me_5)IrCl_2]_2$ with $(Me_3Si)_2S$ in a THF solution affords the $(Ir^{III})_3$ cluster exclusively. The addition of oxidizing equivalents in the form of elemental sulfur to the reaction of $[(C_5Me_5)IrCl_2]_2$ and $(Me_3Si)_2S$ led to a 5-fold increase in the yield of $[\mathbf{1}]^{2+}$ (eq 3).

$$^3/_2[(C_5Me_5)IrCl_2]_2 + 2(Me_3Si)_2S \rightarrow \underset{[\mathbf{2}]^{2+}}{[(C_5Me_5)_3Ir_3S_2]Cl_2} + 4Me_3SiCl \quad (2)$$

$$2[(C_5Me_5)IrCl_2]_2 + 3(Me_3Si)_2S + {}^1/_8S_8 \rightarrow \underset{[\mathbf{1}]^{2+}}{[(C_5Me_5)_4Ir_4S_4]Cl_2} + 6Me_3SiCl \quad (3)$$

Control experiments showed that $[\mathbf{2}]^{2+}$ does not convert to $[\mathbf{1}]^{2+}$ under relevant conditions, for example $[\mathbf{2}]^{2+}$ does not react with sulfiding agents. Thus, it appears that the $[\mathbf{1}]^{2+}/[\mathbf{2}]^{2+}$ distribution is established early in the reaction sequence. The added elemental sulfur employed in the synthesis of $[\mathbf{1}]^{2+}$ is involved at an intermediate mechanistic stage since neither $[\mathbf{1}]^{2+}$ nor $[(C_5Me_5)IrCl_2]_2$ is reactive toward S_8.

Electrochemistry and Redox Reactions. Cyclic voltammetry of a CH_2Cl_2 solution of $[\mathbf{1}]^{2+}$ showed 1 e^- reductions at –218 and –487 mV vs Ag/AgCl (Figure 2A). Scanning to still more positive potentials revealed a possible oxidation to $[\mathbf{1}]^{3+}$ at 930 mV. On the basis of the two $E_{1/2}$'s the conproportionation constant for the formation of $[\mathbf{1}]^+$ from $[\mathbf{1}]^{2+}$ and $[\mathbf{1}]^0$ was calculated to be 90. The i_a/i_c ratios of 0.795 to 0.877 for the two waves suggest electrochemical reversibility (total reversibility at an i_a/i_c ratio of 1). Plots of the square root of the scan rate vs peak current were linear over nine scan rates ranging from 25 to 500 mV indicating that the redox events are diffusion controlled and are not subject to rate limiting structural changes. As suggested by the electrochemical results, solutions of $[\mathbf{1}]^{2+}$ underwent reduction by 2 equiv of $(C_5H_5)_2Co$ affording good yields of neutral $(C_5Me_5)_4Ir_4S_4$ (eq 4).

(7) (a) Schunn, R. A.; Fritchie, C. J., Jr.; Prewitt, C. T. *Inorg. Chem.* **1966**, *5*, 892. (b) Wei, C. H.; Wilkes, G. R.; Treichel, P. M.; Dahl, L. F. *Inorg. Chem.* **1966**, *5*, 900.

(8) In contrast to more recent work on Fe–Se clusters,[8] the crystallographic analysis of $[(RC_5H_4)_4Fe_4S_4]^{2+}$ indicates a partially delocalized structure. Four Fe–Fe contacts of intermediate length (2.8 Å) are observed which Dahl et al. assign to a bond order of $^3/_4$: Trinh-Toan; Teo, B. K.; Ferguson, J. A.; Meyer, T. J.; Dahl, L. F. *J. Am. Chem. Soc.* **1977**, *99*, 408.

(9) (a) Inomata, S.; Tobita, H.; Ogino, H. *Inorg. Chem.* **1992**, *31*, 722. (b) Ogino, H.; Tobita, H.; Yanagisawa, K.; Shimoi, M.; Kabuto, C. *J. Am. Chem. Soc.* **1987**, *109*, 5847.

(10) See for example: Shriver, D. F.; Atkins, P. W.; Langford, C. H. *Inorganic Chemistry*; Freeman: New York, 1990.

(11) (a) Sorai, M.; Kosaki, A.; Suga, H.; Seki, S.; Yoshida, T.; Otsuka, S. *Bull. Chem. Soc. Jpn.* **1971**, *44*, 2364. (b) Otsuka, S.; Nakamura, A.; Yoshida, Y. *Inorg. Chem.* **1968**, *7*, 261. (c) Otsuka, S.; Nakamura, A.; Yoshida, Y. *Justus Liebigs Ann. Chem.* **1968**, *719*, 54. (d) Komijo, N.; Watanabe, T. *Acta Crystallogr.* **1979**, *B35*, 2537. (e) Pulliam, C. R.; Thoden, J. B.; Stacy, A. M.; Spencer, B.; Englert, M. H.; Dahl, L. F. *J. Am. Chem. Soc.* **1991**, *113*, 7398.

(12) Lockemeyer, J. R.; Rauchfuss, T. B.; Rheingold, A. L. *J. Am. Chem. Soc.* **1989**, *111*, 5733.

(13) Koide, Y.; Bautista, M. T.; White, P. S.; Schauer, C. K. *Inorg. Chem.* **1992**, *31*, 3690.

(14) (a) Houser, E. J.; Amarasekera, J.; Rauchfuss, T. B.; Wilson, S. R. *J. Am. Chem. Soc.* **1991**, *113*, 7440. (b) Houser, E. J.; Rauchfuss, T. B.; Wilson, S. R. *Inorg. Chem.* **1993**, *32*, 4069.

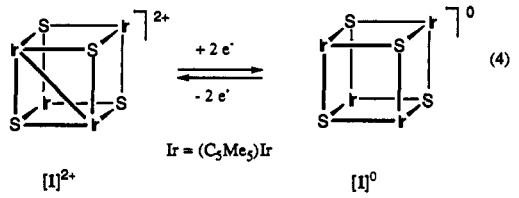

(4)

The ^{1}H NMR spectrum of this red species [1] exhibits a single resonance at 1.72 ppm (C_6D_6), as reported by Dobbs and Bergman who prepared it from $(C_5Me_5)_2Ir_2(\mu_2\text{-}S)_2(PR_3)$.[15] The neutral tetrairidium cluster was cleanly oxidized by HCl in air to give $[1]^{2+}$. While the optical spectrum of neutral [1] is featureless at wavelengths above 338 nm, solutions of $[1]^{2+}$ are green as indicated by a rather strong absorption at 636 nm, log ϵ = 1.99 (Figure 3).

Cyclic voltammetric studies on CH_2Cl_2 solutions of $[2]^{2+}$ revealed 1 e$^-$ reductions at −712 and −993 mV (Figure 2B). Measurements out to 1.5 V failed to show evidence for further oxidation to the Ir^{IV} level. The i_a/i_c ratios of 0.911 to 0.920 for the two waves indicate electrochemical reversibility. The dependence of the square root of the scan rate vs the peak current over scan rates ranging from 25 to 500 mV was found to be linear. The conproportionation constant for the formation of $[2]^+$ from $[2]^{2+}$ and $[2]^0$ is 117. Reduction of $[2]^{2+}$ using 2 equiv of $(C_5H_5)_2Co$ gave the extremely air sensitive neutral derivative $[(C_5Me_5)_3Ir_3S_2]^0$, $[2]^0$ (eq 5).

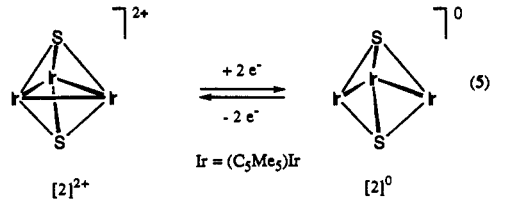

(5)

The deep blue color of this mixed valence cluster results from a strong absorbance at 592 nm (log ϵ = 2.28), in contrast to the pale yellow color of $[2]^{2+}$ (λ_{max} = 344 nm) (Figure 4). Results of the electrochemical studies are presented in Table 1.

NMR Studies of $[(C_5Me_5)_4Ir_4S_4]^z$. The ^{1}H NMR spectrum of $[1]^0$ consists of a singlet at 1.72 ppm. It appears that the four Ir centers are equivalent as confirmed by the crystal structure analysis described by Bergman and Dobbs.[15] In contrast, the room temperature ^{1}H NMR spectrum of $[1]^{2+}$ suggested dynamic behavior since it consisted of a very broad singlet (Figure 5). Essentially the same spectrum is observed for aqueous solutions of $[1]Cl_2$ and for CD_3CN and CD_2Cl_2 solutions of $[1](PF_6)_2$. Variable-temperature measurements revealed that the broad singlet sharpened at higher temperatures and split into two sharp singlets at low temperatures. At 400 MHz the coalescence temperature was 13 °C corresponding to $\Delta G^{\ddagger}$ of 57 kJ/mol, according to the Gutowsky–Holm relationship.[16] The NMR spectra were digitally simulated over a range of temperature from −37 to 38 °C. There is a slight temperature dependence of the chemical shifts in the experimental spectra; however, the chemical shift difference of the two exchanging sites was assumed to be temperature independent for the simulation. The simulations yielded the following activation parameters: $\Delta H^{\ddagger}$ = 80 ± 10 kJ/mol and $\Delta S^{\ddagger}$ = 82 ± 36 J/(mol K). These values give a calculated $\Delta G_{298}{}^{\ddagger}$ value of 56 ± 15 kJ/mol, which is in agreement with the calculation from the coalescence temperature. The ^{13}C-{^{1}H} NMR spectrum at −50 °C showed two pairs of resonances corresponding to two sets of nonequivalent C_5Me_5 groups (Figure 6A). The exchange rates for $[(C_5Me_5)_4Ir_4S_4]^{2+}$ were found to be independent of concentration, hence they are associated with an intramolecular process.

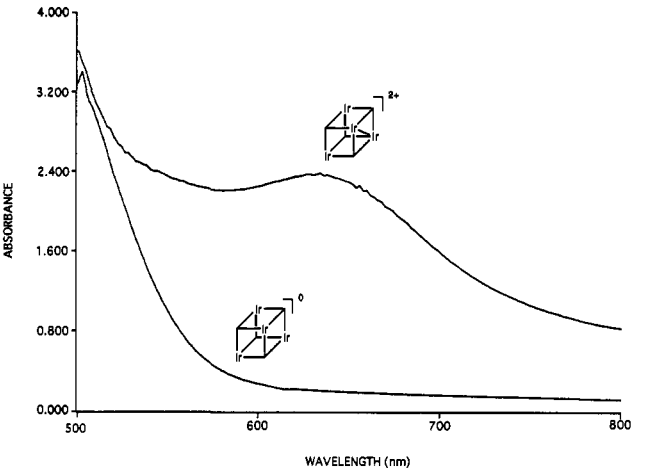

Figure 3. Absorption spectra of 2.45 × 10^{-3} M (CH_3CN) solutions of $[(C_5Me_5)_4Ir_4S_4](PF_6)_2$ (A) and $(C_5Me_5)_4Ir_4S_4$ (B).

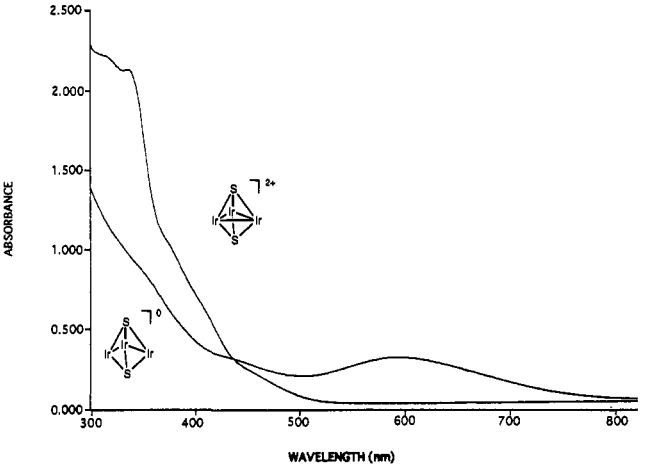

Figure 4. Absorption spectra of 1.63 × 10^{-4} M (CH_3CN) solutions of $[(C_5Me_5)_3Ir_3S_2](PF_6)_2$ (A) and $(C_5Me_5)_3Ir_3S_2$ (B).

Table 1. Electrochemical Data for $[1]^z$ and $[2]^z$ at Scan Rates of 100 mV s^{-1}

compd	$E_{pa}(1)^a$ (mV)	$E_{pc}(1)^a$ (mV)	i_a/i_c	$E_{pa}(2)^a$ (mV)	$E_{pc}(2)^a$ (mV)	i_a/i_c
$[(C_5Me_5)_4Ir_4S_4]^z$	−252	−317	0.80	−515	−587	0.88
$[(C_5Me_5)_3Ir_3S_2]^z$	−679	−745	0.91	−957	−1029	0.93

^{a} $E_{pa}(1)$ and $E_{pc}(1)$ refer to the peak potentials of the anodic and cathodic waves, respectively.

Methylated ligands are particularly well suited for ^{13}C NMR analysis in the solid state by CP-MAS techniques. The spectrum of a solid sample of $[(C_5Me_5)_4Ir_4S_4](PF_6)_2$ was examined to demonstrate the rigidity of the metal–metal bond in the solid state. In the methyl region, the resonances at 9.99 and 9.25 ppm were assigned to the two sets of nonequivalent $C_5\mathit{Me}_5$ groups, while in the aromatic region a signal at 95.68 and a pair of signals at 105.23 and 106.89 ppm were observed. The pair of closely spaced high frequency signals are assigned to the $(C_5Me_5)Ir$ sites which are slightly nonequivalent due to the low crystallographic site symmetry (Figure 6B). For comparison, the solid-state CP-MAS spectrum of $[1]^0$ has a singlet at 8.98 for the methyl carbons and a singlet at 88.98 ppm for the aromatic carbons, corresponding to equivalent C_5Me_5 groups. These measurements suggest that the low-field C_5Me_5 signal at 95.68 ppm in the spectrum of $[1]^{2+}$ is associated with Ir^{III} sites.

NMR Studies of $[(C_5Me_5)_3Ir_3S_2]^z$. The 400-MHz ^{1}H NMR spectrum of a CD_3CN solution of $[2]^{2+}$ consists of a sharp singlet

(15) Dobbs, D. A.; Bergman, R. G. *J. Am. Chem. Soc.* **1992**, *114*, 6908.
(16) (a) Gutowsky, H. S.; Holm, C. H. *J. Chem. Phys.* **1956**, *25*, 1228. (b) Ebsworth, E. A. V.; Rankin, D. W. H.; Cradock, S. *Structural Methods in Inorganic Chemistry*; CRC: New York, 1991.

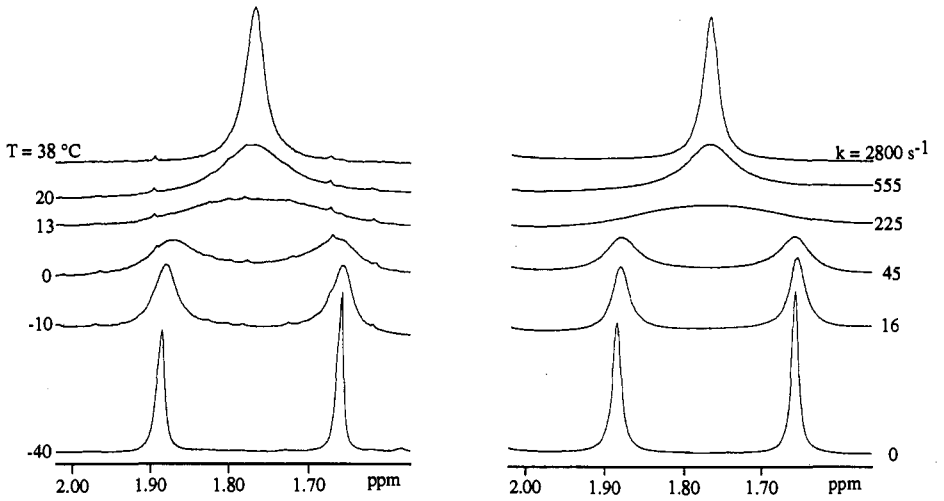

Figure 5. Experimental and simulated variable-temperature 400-MHz ^{1}H NMR spectra of $[(C_5Me_5)_4Ir_4S_4](PF_6)_2$ (CD_2Cl_2 solution).

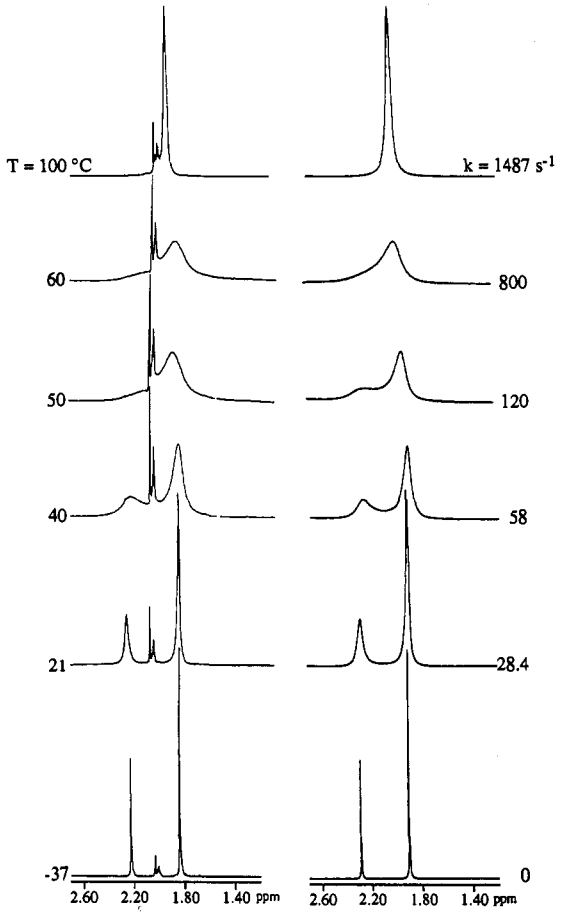

Figure 6. Experimental and simulated variable-temperature 400-MHz ^{1}H NMR spectra of $[(C_5Me_5)_3Ir_3S_2]$ ($C_6D_5CD_3$ solution). The singlet at ~2 ppm is due to an impurity.

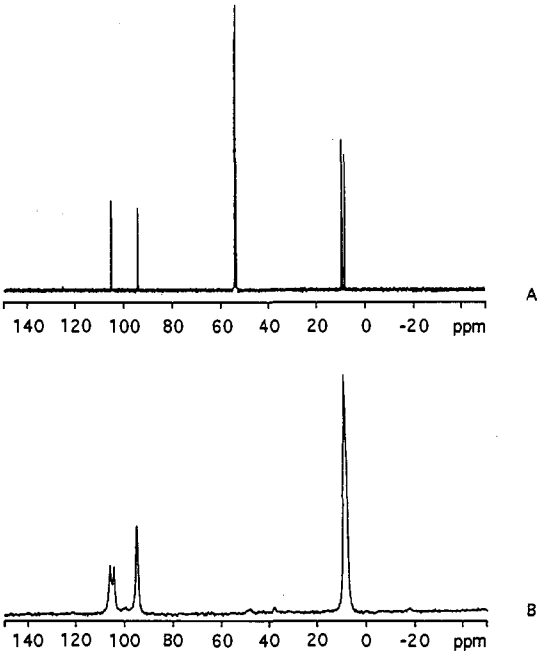

Figure 7. ^{13}C $\{^1$H$\}$ 100-MHz NMR spectrum of a CD_2Cl_2 solution of $[(C_5Me_5)_4Ir_4S_4](PF_6)_2$ (−50 °C) (A). ^{13}C$\{^1$H$\}$ CP-MAS 75.5-MHz NMR spectrum of microcrystalline $[(C_5Me_5)_4Ir_4S_4](PF_6)_2$ (B).

at 2.24 ppm indicative of equivalent C_5Me_5 groups. The ^{13}C$\{^1$H$\}$ NMR spectrum consists of only one signal each for the methyl and ring carbons of the C_5Me_5 ligands. In contrast, the room temperature ^{1}H NMR spectrum of $[\mathbf{2}]^0$ featured two broad singlets (Figure 7). At 60 °C these peaks coalesce and at 100 °C the spectrum consists of a sharp singlet. The limiting low-temperature ^{1}H NMR spectrum (−37 °C) consists of two sharp singlets with integrated intensities of 2:1. These DNMR data were digitally simulated over a temperature range of −37 to 100 °C. The simulations gave activation parameters of $\Delta H^* = 43 \pm 5$ kJ/mol and $\Delta S^* = -72 \pm 15$ J/(mol K) with $\Delta G^* = 64 \pm 7$ kJ/mol (298 K).

Crystallographic Studies on $[(C_5Me_5)_4Ir_4S_4](PF_6)_2$. The salt features a distorted cuboidal $(C_5Me_5)_4Ir_4S_4$ cluster with well-separated PF_6^- counterions, as well as two molecules of acetone. Crystallographic symmetry was not imposed on the cations. Of interest are the nature and the degree of the deviations of the Ir_4 core from tetrahedral symmetry (Figure 8, Table 2). The cluster is distorted by virture of the short Ir(2)–Ir(3) contact of 2.764(1) Å resulting in a Ir_4 core of idealized C_{2v} symmetry. These two iridium centers are assigned to the Ir^{IV} oxidation state and the short distance is interpreted as a direct metal–metal bond. For comparison the Ir–Ir bonding distance in iridium metal is 2.71 Å[17] while the still more appropriate structural model $Ir_4(CO)_{12}$ has Ir–Ir contacts of 2.69 Å.[18] The four $Ir^{III}\cdots Ir^{IV}$ contacts (3.563(1)–3.586(1) Å) are assigned as nonbonding. For comparison the six Ir···Ir contacts in the parent 72 e$^-$ cluster $(C_5R_5)_4Ir_4S_4$ fall in the narrow range of 3.584–3.602 Å. The unique $Ir^{III}\cdots Ir^{III}$ interaction in $[\mathbf{1}]^{2+}$ has the longest contact of 3.683(1) Å. The

(17) (a) *CRC Handbook of Chemistry and Physics*, 69th ed.; Weast, R. C., Ed.; CRC: Cleveland, 1988; p F-166. (b) Bondi, A. *J. Phys. Chem.* **1964**, *68*, 441.
(18) Churchill, M. R.; Hutchinson, J. P. *Inorg. Chem.* **1978**, *17*, 3528.

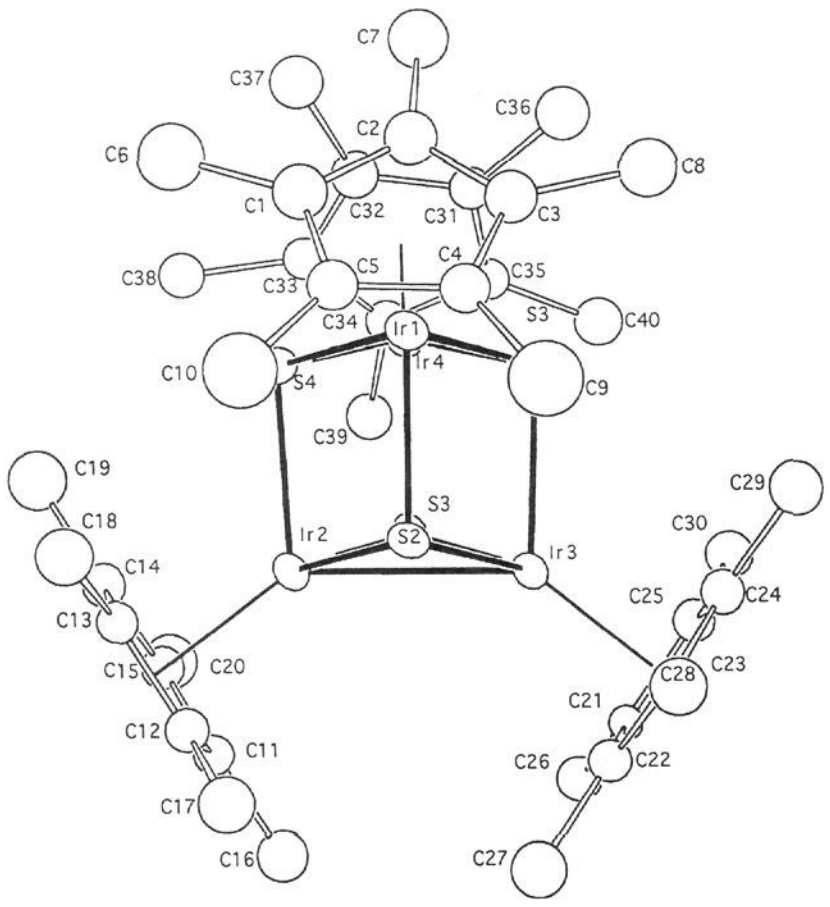

Figure 8. ORTEP drawing of the dication in $[(C_5Me_5)_4Ir_4S_4[(PF_6)_2$ with the non-hydrogen atoms removed for clarity.

Table 2. Selected Bond Distances (Å) and Angles (deg) for $[(C_5Me_5)_4Ir_4S_4](PF_6)_2$ ($[\mathbf{1}]^{2+}$)

Ir1–Ir2	3.565(1)	Ir1–Ir2	3.567(1)
Ir1–Ir4	3.683(1)	Ir2–Ir3	2.764(1)
Ir2–Ir4	3.563(1)	Ir3–Ir4	3.568(1)
S1–S2	3.632(7)	S1–S3	33.023(8)
S1–S4	3.079(7)	S2–S3	3.101(7)
S2–S4	3.063(7)	S3–S4	2.991(7)
Ir2–S1	2.325(5)	Ir3–S1	2.308(5)
Ir4–S1	2.308(5)	Ir1–S2	2.329(5)
Ir2–S2	2.329(5)	Ir3–S2	2.330(5)
Ir1–S3	2.413(5)	Ir3–S3	2.384(5)
Ir4–S3	2.385(5)	Ir1–S4	2.386(5)
Ir2–S4	2.378(5)	Ir4–S4	2.409(5)
S–Ir^{IV}–S	80.2(2)–103.1(2)	S–Ir^{III}–S	77.1(2)–81.7(2)
Ir^{III}–S–Ir^{III}	100.3(2)–100.4(2)	Ir^{IV}–S–Ir^{IV}	73.1(2)–73.3(1)
Ir^{III}–S–Ir^{IV}	96.1(2)–101.9(2)		

bonding Ir^{III}–S (2.308(5)–2.413(5) Å) and Ir^{IV}–S (2.308(5)–2.384(5) Å) distances are quite similar.

Using molecular modeling techniques we examined the possibility of close H···H contacts in $[\mathbf{1}]^{2+}$. Hydrogen atom positions were calculated on the basis of idealized tetrahedral methyl carbon centers and the methyl groups were rotated so as to bring the H atoms into closest contact. The closest H···H contact is 1.23 Å between methyl groups on two Ir^{IV} centers. The van der Waals radius for hydrogen is 1.2 Å.[17] Although these calculations show that these methyl groups can clash sterically, they overstate any problems since other methyl rotamers show H···H contacts beyond the van der Waals range.

Crystallographic Studies on $[(C_5Me_5)_3Ir_3S_2](PF_6)_2$. The salt features a roughly trigonal bipyramidal Ir_3S_2 core with well-separated PF_6^- counterions as well as one acetone molecule. Crystallographic symmetry was not imposed on the cation (Figure 10, Table 3). The three Ir–Ir bonds are nearly equivalent (2.8201(7)–2.8157(7) Å) as are the Ir–S distances (2.275(3)–2.294(3) Å). The degree of pyramidalization at sulfur is indicated by the Ir–S–Ir angles (76.0–76.46°) which are larger than those of the cobalt analog $[(C_5H_4Me)_3Co_3S_2](SbF_6)_2$ with Co–S–Co angles of 71.6 to 74°.[11e] A space-filling diagram demonstrates the decreased crowding in the Ir_3S_2 molecule, with closest H···H contacts of 1.98 Å between C_5Me_5 groups and 1.66 Å between H atoms within a given C_5Me_5 ligand (Figure 11).

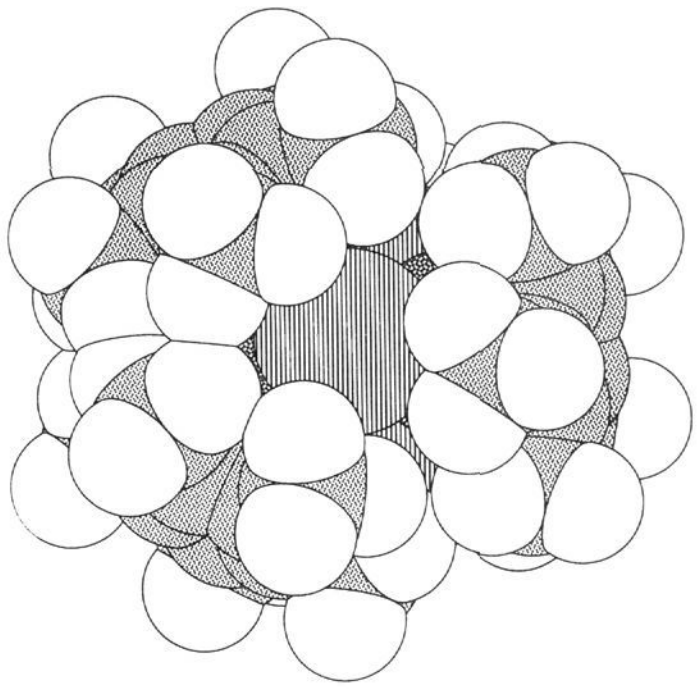

Figure 9. Space filling model of the dication in $[(C_5Me_5)_4Ir_4S_4](PF_6)_2$. Hydrogen positions were calculated. The following van der Waals radii (Å) were used for this drawing: C, 1.60; H, 1.20; Ir, 2.30; S, 1.85. The Ir atoms are stipled.

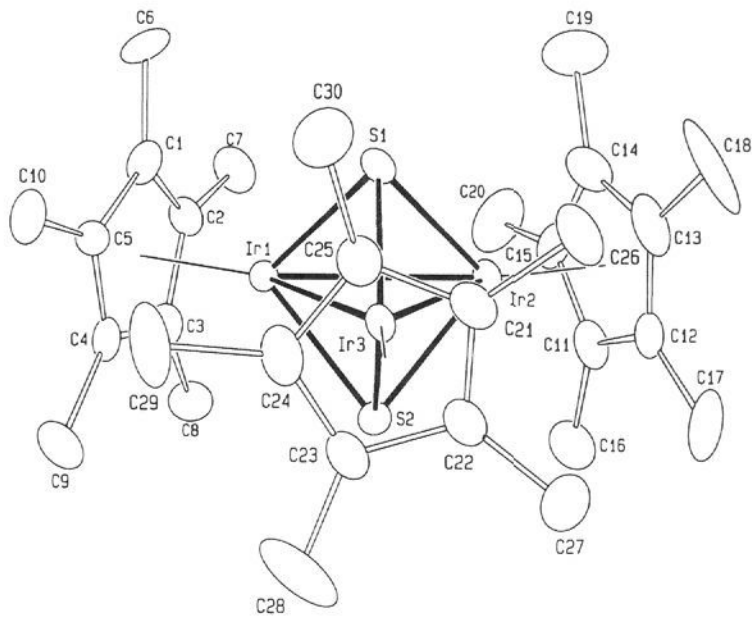

Figure 10. *ORTEP drawing of the dication in* $[(C_5Me_5)_3Ir_3S_2](PF_6)_2$ with the non-hydrogen atoms removed for clarity.

Table 3. Selected Bond Distances (Å) and Angles (deg) for $[(C_5Me_5)_3Ir_3S_2](PF_6)_2$ ($[\mathbf{2}]^{2+}$)

Ir1–Ir2	2.8201(7)	Ir1–Ir3	2.8157(7)
Ir2–Ir3	2.8169(7)	Ir1–S1	2.283(3)
Ir2–S1	2.277(3)	Ir3–S1	2.275(3)
Ir1–S2	2.275(3)	Ir2–S2	2.294(3)
Ir3–S2	2.280(3)	S1–S2	3.197(5)
Ir2–Ir1–Ir3	59.98(2)	Ir1–S1–Ir2	76.4(1)
Ir1–S1–Ir3	76.29(10)	Ir2–S1–Ir3	76.46(10)
Ir1–S2–Ir2	76.2(1)	Ir1–S2–Ir3	76.4(10)
Ir2–S2–Ir3	76.0(1)		

Discussion

This project was developed to prepare and examine clusters exhibiting mobile metal–metal bonds. Our efforts were rewarded by a one-pot route to two types of clusters which exhibit this property. Specifically, $[(C_5Me_5)IrCl_2]_2$ was found to react with a mixture of $(Me_3Si)_2S$ and elemental sulfur to give both $[(C_5Me_5)_3Ir_3S_2]^{2+}$ and $[(C_5Me_5)_4Ir_4S_4]^{2+}$. We propose that the two clusters arise via the initial formation of $(C_5Me_5)_2Ir_2(\mu_2\text{-}S)_2$. This same species has been invoked previously in the thermal condensation of $(C_5Me_5)_2Ir_2(\mu_2\text{-}S)_2(PMe_3)$ to give $(C_5Me_5)_4Ir_4S_4$ with loss of phosphine.[15] Conceivably the Ir_3S_2 cluster arises by the complexation of $(C_5Me_5)_2Ir_2(\mu_2\text{-}S)_2$ with $(C_5Me_5)IrCl_2$ followed by loss of chloride. The formation for the mixed valence cubane cluster is not as easily explained, although our control

experiments suggest that it is an intermediate not the starting or final product which reacts with the added sulfur. It seems likely that $(C_5Me_5)_2Ir_2(\mu_2\text{-}S)_2$ would be reactive toward sulfur to give persulfido species.[19]

As seen for many other cyclopentadienyl metal sulfide clusters, both $[\mathbf{1}]^0$ and $[\mathbf{2}]^0$ undergo redox reactions under conditions that are electrochemically addressable. The results of cyclic voltammetry experiments guided the selection of redox agents employed to generate the mixed valence clusters. Within the context of mononuclear chemistry there is no simple explanation for the nature of the redox processes observed. In one case, the low potential processes interrelate Ir^{III} and Ir^{IV} states while in the second case it is the Ir^{II} and Ir^{III} states that are addressed. In each case we observe two redox events which are well separated in potential. In this regard these Ir species differ from related Ru_3S_2 and Ru_4S_4 clusters where the two redox steps are separated by <100 mV.[11,13] The crystallographic results show that the net effect of the two redox steps is the making or breaking of Ir–Ir bonds. The reversible formation/destruction of metal–metal bonds in bimetallic complexes is well-known when the two metals are constrained by a ligand bridge.[20] The unusual aspect of $[\mathbf{1}]^{2+}$ and $[\mathbf{2}]^0$ is that the metal–metal bonds are situated in frameworks that allow the degenerate hopping of the bond or nonbond.

The species $[(C_5R_5)_4Ir_4S_4]^{2+}$ is an unusual example of a cuboidal cluster with only one M–M bond. It represents a new member of the series of clusters presented in Figure 1. Within this family of clusters, those with cluster electron counts not divisible by four are necessarily mixed valence and are potentially subject to degenerate relocation of the metal–metal bond. Indicative of the mixed valence character of $[\mathbf{1}]^{2+}$ is the appearance of a strong low-energy electronic band in contrast to the featureless visible spectrum of the neutral homovalent cluster.

Iridium(IV) compounds are typically associated with electronegative ligands which are capable of ligand-to-metal π-donation, such as $IrCl_6^{2-}$.[21] Ir^{IV} is also known to be stabilized by strongly donating organic ligands as in $[(C_5Me_5)_2Ir_2(\mu\text{-}CH_2)_2\text{-}Cl_2]$.[22] Cluster $[\mathbf{1}]^{2+}$ stands however as a unique example of an Ir^{IV} sulfide. The mineral IrS_2[24] adopts a pyrite structure formally comprised of Ir^{II} and persulfides, in contrast to $IrTe_2$ which crystallizes in the CdI_2 motif with isolated Te^{-II} and Ir^{IV} units.[24] The first reported Ir cluster, $Ir_3N(SO_4)_6(H_2O)_3^{4-}$ ("Delepine's green salt"), is formally described as $(Ir^{IV})_2(Ir^{III})$ although the highly symmetric structure of this diamagnetic species suggests a delocalized ground state.[25] It is very likely that N or Ir π-bonding plays a significant role in the stabilization of this species, especially since the Ir···Ir separations are beyond bonding distances.

The trimetallic cluster $[(C_5Me_5)_3Ir_3S_2]^{2+}$ is a highly symmetrical species featuring three Ir–Ir bonding interactions. Reduction of this species to the mixed valence $(Ir^{II})_2Ir^{III}$ cluster is also accompanied by the appearance of a strong absorption band in the visible region. The solid-state structure of this species was not determined; however, it was assumed to be analogous to $[(cymene)_3Ru_3S_2]^0$, which was characterized by single crystal X-ray diffraction.[11] This $Ru^{II}Ru^{I}_2$ cluster adopts an idealized C_{2v} core as seen for other five-vertex, 50 e$^-$ clusters.[12] The present results suggest that this Ru_3 cluster may also exhibit dynamics associated with mobile Ru–Ru bonds.

(19) Wachter, J. *Angew. Chem., Int. Ed. Engl.* **1989**, *28*, 1613; *Angew. Chem.* **1989**, *12*, 1645.

(20) (a) Mueller-Westerhoff, U. T.; Rheingold, A. L.; Swiegers, G. F. *Angew. Chem., Int. Ed. Engl.* **1992**, *31*, 1352; *Angew. Chem.* **1992**, *104*, 1398. (b) Connelly, N. G.; Lucy, A. R.; Payne, J. D.; Galas, A. M. R.; Geiger, W. E. *J. Chem. Soc., Dalton Trans.* **1983**, 1879.

(21) Vasquez de Miguel, A.; Isobe, K.; Taylor, B. F.; Nutton, A.; Maitlis, P. M. *J. Chem. Soc., Chem. Commun.* **1982**, 758.

(22) Kauffman, G. B.; Myers, R. D. *Inorg. Synth.* **1966**, *8*, 223.

(23) (a) Brown, D. B.; Robin, M. B.; McIntyre, J. D. E.; Peck, W. F. *Inorg. Chem.* **1970**, *10*, 2315. (b) Ciechanowicz, M.; Griffith, W. P.; Pawson, D.; Skapski, A. C.; Cleare, M. J. *J. Chem. Soc., Chem. Commun.* **1971**, 876.

(24) Hulliger, F. *Struct. Bonding* **1978**, *4*, 83–229.

(25) Delepine, M. *Ann. Chim.* **1959**, *13*, 1115.

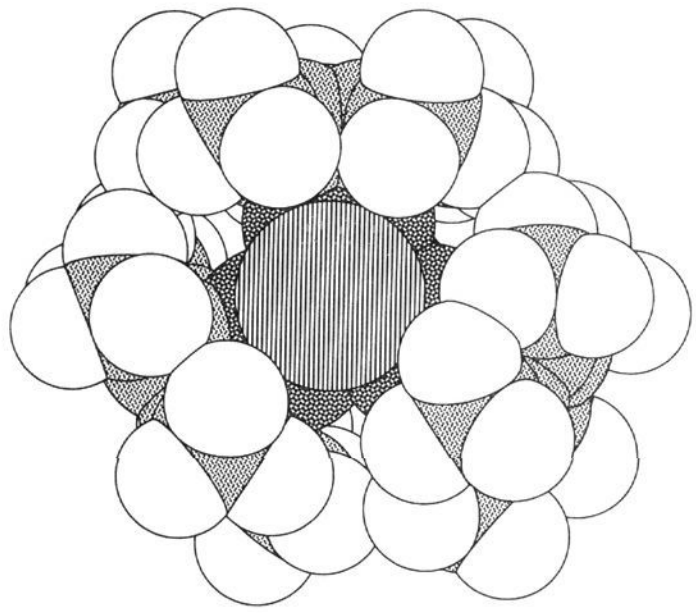

Figure 11. Space filling diagram of the dication in $[(C_5Me_5)_3Ir_3S_2](PF_6)_2$. Hydrogen positions were calculated. The following van der Waals radii (Å) were used for this drawing: C, 1.60; H, 1.20; Ir, 2.30; S, 1.85. The Ir atoms are stipled.

The DNMR studies demonstrate the mobility of the metal–metal bonds in $[\mathbf{1}]^{2+}$ and $[\mathbf{2}]^0$. The DNMR patterns are consistent with the movement of one bond or one nonbond as in the case of $[\mathbf{2}]^0$. The rates are first order and the dynamics are intramolecular since the barriers are independent of concentration. CP-MAS measurements on $[\mathbf{1}](PF_6)_2$ indicate that the cluster core is rigid in the solid state. This is expected since the crystallographic studies show that the single Ir–Ir bond is associated with a substantial distortion of the Ir_4 core from tetrahedral symmetry. Thus the shift of the Ir–Ir bond entails the elongation of one bond by 0.9 Å and the contraction of one bond by the same amount, as well as 0.1 Å changes associated with the shift of the Ir^{III}···Ir^{III} contact. Such motion is not expected to occur in a solid where many of the atomic positions are constrained by electrostatic and van der Waals forces.

The mechanism by which the Ir–Ir bonds and nonbonds migrate among the equivalent sites has not been established. The disparate values of the entropies of activation (+82 ± 36 J/(mol K) for $[\mathbf{1}]^{2+}$ and –72 ± 15 J/(mol K) for $[\mathbf{2}]^0$) for the dynamics of $[\mathbf{1}]^{2+}$ and $[\mathbf{2}]^0$ are difficult to explain. In the case of $[\mathbf{1}]^{2+}$, the stepwise relocation of the Ir–Ir (non)bonding interaction to an adjacent edge can be effected via electron transfer from one of two Ir^{III} centers to one of two Ir^{IV} sites (eq 6).

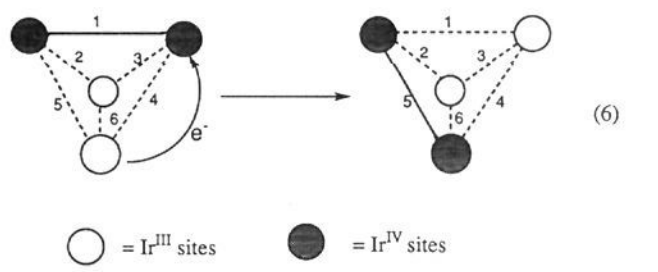

(6)

There are four equivalent pathways for such a process. According to this mechanism it is not possible to relocate the Ir–Ir bond in one step across the body center of the Ir_4 tetrahedron. The corresponding mechanism for the Ir_3 cluster invokes electron transfer from one of two Ir^{II} to the unique Ir^{III} center (eq 7).

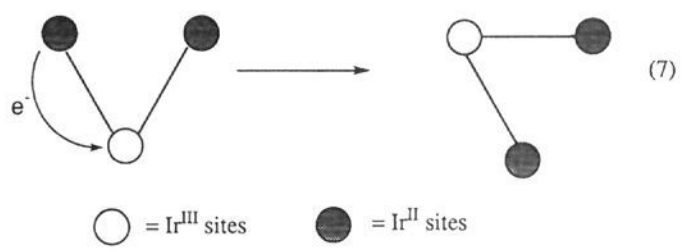

(7)

These aforementioned mechanisms are simplified in that they focus exclusively on the metal–metal bonds. Furthermore our

description relies on assignments of formal oxidation states. An alternative description of these dynamics can be developed on the basis of molecular orbital theory. For example, Fenske and coworkers have discussed the relationship between the electron counts and geometry of organometallic M_3S_2 clusters.[26] On the basis of molecular orbital calculations the D_{3h} core structures of 48 e⁻ clusters like $[2]^{2+}$ can be rationalized, with the HOMO consisting of nonbonding t_{2g}-like orbitals centered on the metals. For the corresponding 50 e⁻ clusters such as $[2]^0$, the two added electrons would occupy orbitals that transform as e′ and a′. This configuration would be subject to a Jahn–Teller distortion to give a cluster with C_{2v} symmetry. Under this reduced symmetry, the HOMO then transforms as b_2 and is doubly occupied. If one accepts this model, then the barrier controlling the dynamics in $[2]^0$ is a measure of the stabilization resulting from the Jahn–Teller distortion.[27]

The present work provides particularly simple examples of mobile metal–metal bonds in cluster frameworks. There are still only a few examples of this phenomenon, and the factors that control the energetics are not well understood. Experiments designed to probe the mechanism of the dynamics are underway.

Experimental Section

Materials. The hydrated trichloride of iridium was obtained from Johnson Matthey. $[(C_5Me_5)IrCl_2]_2$[28] and $(Me_3Si)_2S$ (Caution: STENCH!),[29] were prepared according to literature methods. $(C_5H_5)_2Co$ (Aldrich) was vacuum sublimed at 40 °C. Tetrahydrofuran, benzene, and hexanes were distilled from Na/K alloy. Dichloromethane and acetonitrile were distilled from CaH_2. Methanol (Fischer) was used as received. All solvents were deoxygenated with dry O_2-free nitrogen.

Methods. Elemental analyses were performed by the University of Illinois Microanalytical Laboratory. Positive ion FAB mass spectra were recorded on a VG ZAB-SE instrument at the SCS Mass Spectrometry Laboratory using the "Magic Bullet" matrix (3:1 mixture of dithioerythritol–dithiothreitol). The results are reported for ^{193}Ir. Solution ^1H and ^{13}C NMR spectra were recorded on a Varian U400 spectrometer while CP-MAS measurements employed a GE WB 300-MHz instrument. UV–vis spectra were measured on a Hewlett Packard 8452A spectrometer using a 1 cm path length quartz cell. The data are reported with λ_{max} in nm ($\log \epsilon$ in $M^{-1}\,cm^{-1}$). Preparative operations, unless otherwise stated, were performed under an atmosphere of nitrogen using standard Schlenk techniques.

Electrochemistry. Electrochemical experiments were carried out on a Bioanalytical Systems BAS-100 electrochemical analyzer. Cyclic voltammograms were measured on $\sim 10^{-3}$ M CH_2Cl_2 solutions with 0.1 M n-Bu_4NPF_6 as the supporting electrolyte and Pt working and counter electrodes vs Ag/AgCl. Under these conditions, the $(C_5H_5)_2Fe^{0/+}$ couple was +572 mV (ΔE_p = 85 mV). To calculate conproportionation constants (K_c), $E_{1/2}$'s were taken as $E°_1$ and $E°_2$ the for the two redox events[30] ($E°$ = $(E_{pc} + E_{ac})/2$).

$$K_c = \exp[(E°_1 - E°_2)n_1n_2F/RT] = ([\mathbf{1}]^+)^2/([\mathbf{1}]^{2+})([\mathbf{1}]^0) = 90$$

Dynamic NMR Simulations. The free energy of activation can be calculated from the coalescence temperature (T_c) and $\Delta\nu$, the separation (in Hz) between the two signals via the following equations.[31]

$$k_c = 2.22\Delta\nu$$

$$\Delta G_c^{\ddagger} = 19.14T_c[10.32 + T_c/k_c]\ \text{J/mol}$$

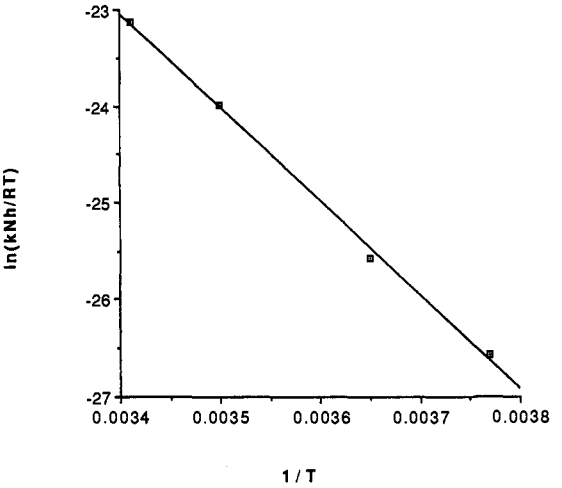

Figure 12. Eyring plot of the rate data from the simulated variable-temperature ^1H NMR spectra (400 MHz) of $[(C_5Me_5)_4Ir_4S_4](PF_6)_2$.

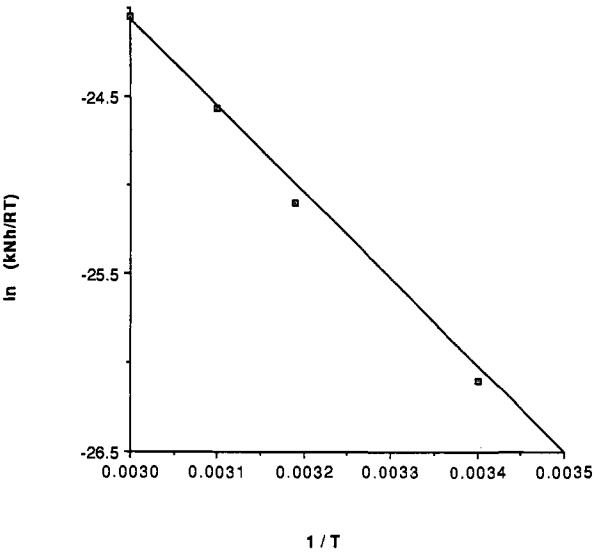

Figure 13. Eyring plot of the rate data from the simulated variable-temperature ^1H NMR spectra (400 MHz) of $(C_5Me_5)_3Ir_3S_2$.

DNMR simulations were carried out on a VAX station using the program DNMR3.[32] The rate constants for various temperatures were obtained by visually matching observed and calculated spectra. For the calculation of activation parameters, we included only data for the spectra that exhibited significant line broadening of ~2 Hz more than the fast exchange line width (inclusion of data beyond the fast and slow exchange limits results in far better fits to the Eyring plots but the simulations for these rate regimes are unreliable). The transverse relaxation times (T_2 = π^{-1} (line width)$^{-1}$) for $[\mathbf{1}]^{2+}$ were 0.065 and 0.082 s^{-1} for the signals at 1.886 and 1.657 ppm, respectively. In the case of $[2]^0$, the T_2's were 0.180 and 0.176 s^{-1} for the 2.306- and 1.919-ppm signals, respectively. Activation energies were obtained from plots of $\ln(k_{obs}Nh/RT)$ vs $1/T$, where N is 6.02×10^{-23}, $h = 6.63 \times 10^{-34}$ J·s, and $R = 8.32$ J·mol^{-1}·K^{-1}. The plots were linear over the temperature range 265–293 K for $[\mathbf{1}]^{2+}$ and 294–333 K for $[2]^0$ with correlation coefficients of 0.998 for $[\mathbf{1}]^{2+}$ and 0.999 for $[2]^0$. These Eyring plots give slopes of $-\Delta H^{\ddagger}/R$ and y-intercept values of $\Delta S^{\ddagger}/R$ (Figures 12 and 13). Error analysis assumed a 10% error in the rate constant. The temperature of the NMR probe had been previously calibrated using a methanol standard and the error in temperature was estimated at 1 K. Errors were computed by Girolami's method.[33]

(26) Rives, A. B.; Xiao-Zeng, Y.; Fenske, R. F. *Inorg. Chem.* **1982**, *21*, 2286.
(27) A further refinement of this model could consider a singlet D_{3h} transition state (or intermediate) where the configuration of the HOMO is $(e')^2$ or $(a')^2$.
(28) White, C.; Yates, A.; Maitlis, P. M. *Inorg. Synth.* **1992**, *29*, 230.
(29) Armitage, D. A.; Clark, M. J.; Sinden, A. W.; Wingfield, J. N.; Abel, E. W.; Louis, E. J. *Inorg. Synth.* **1974**, *15*, 207.
(30) Strobel, H. A.; Heineman, W. R. *Chemical Instrumentation: A Systematic Approach*; John Wiley: New York, 1089, p 1116.
(31) Friebolin, H. *Basic One- and Two Dimensional NMR Spectroscopy*; VCH: Weinheim, 1991; p 271.
(32) Binsch, G.; Kleier, D. A. *The Computation of Complex Exchange-Broadened NMR Spectra Computer Program DNMR*: QCPE Program No. 140, 1969; Quantum Chemistry Program Exchange, Indiana University.
(33) Morse, P. M.; Spencer, M. H.; Wilson, S. R.; Girolami, G. S. *Organometallics* **1994**, *13*, 1646–1655.

$$(\sigma\Delta H^{\ddagger})^2 = \frac{R^2 T_{max}^{\ 2} T_{min}^{\ 2}}{\Delta T^2}\left\{\left(\frac{\sigma T}{T}\right)^2\left[\left(1 + T_{min}\frac{\Delta L}{\Delta T}\right)^2 + \left(1 + T_{max}\frac{\Delta L}{\Delta T}\right)^2\right] + 2\left(\frac{\sigma k}{k}\right)^2\right\}$$

$$(\sigma\Delta S^{\ddagger})^2 = \frac{R^2}{\Delta T^2}\left\{\left(\frac{\sigma T}{T}\right)^2\left[T_{max}^{\ 2}\left(1 + T_{min}\frac{\Delta L}{\Delta T}\right)^2 + T_{min}^{\ 2}\left(1 + T_{max}\frac{\Delta L}{\Delta T}\right)^2\right] + \left(\frac{\sigma k}{k}\right)^2(T_{max}^{\ 2} + T_{min}^{\ 2})\right\}$$

where $\Delta T = (T_{max} - T_{min})$ and $\Delta L = [\ln(k_{max}/T_{max}) - \ln(k_{min}/T_{min})]$.

Reaction of $[(C_5Me_5)IrCl_2]_2$ with $(Me_3Si)_2S$. (a) In methanol–THF: A slurry of 0.752 g (0.944 mmol) of $[(C_5Me_5)IrCl_2]_2$ in 90 mL of THF and 20 mL of CH_3OH was treated with 0.3 mL (1.43 mmol) of $(Me_3Si)_2S$. The orange reaction mixture was heated under reflux for 48 h. The resulting brown solution was evaporated to dryness. The green-brown crude product was extracted into ~200 mL of H_2O, filtered to remove a brown residue, and loaded onto a 10 × 1 cm column of Sephadex CM-25 cation exchange resin (Na form). Elution with 0.05 M NaCl gave a yellow band followed by a green band. Addition of 2 g (10.9 mmol) of KPF_6 to each of these fractions resulted in the precipitation of the green and yellow salts which were extracted into ~100 mL of CH_2Cl_2. These CH_2Cl_2 solutions were concentrated to ~20 mL and diluted with 50 mL of hexanes to give 0.030 g of $[(C_5Me_5)_4Ir_4S_4](PF_6)_2$, **[1]**$(PF_6)_2$ (4%), and 0.457 g of $[(C_5Me_5)_3Ir_3S_2](PF_6)_2$, **[2]**$(PF_6)_2$ (54%).

(b) In methanol–THF with added sulfur: A mixture of 0.469 g (0.589 mmol) of $[(C_5Me_5)IrCl_2]_2$ and 9.4 mg (0.294 mmol) of S_8 was slurried in 70 mL of THF and 20 mL of methanol and then treated with 0.185 mL (0.883 mmol) of $(Me_3Si)_2S$. The mixture was refluxed for 48 h, resulting in a brown solution. The crude product was extracted into H_2O and purified as above, resulting in 0.1087 g of **[1]**$(PF_6)_2$ (22%) and 0.177 g of **[2]**$(PF_6)_2$ (38%).

(c) In THF: A slurry of 0.50 g (0.628 mmol) of $[(C_5Me_5)IrCl_2]_2$ in 90 mL of THF was treated with 0.176 mL (0.838 mmol) of $(Me_3Si)_2S$. The mixture was refluxed for 25 h, resulting in a color change from orange to yellow orange. The crude product was extracted into ~200 mL of H_2O and filtered to remove a brown residue. The filtrate was worked up as above to give 0.272 g of **[2]**$(PF_6)_2$ (47% yield).

(d) In THF, with added sulfur: A slurry of 0.50 g (0.628 mmol) of $[(C_5Me_5)IrCl_2]_2$ and 10 mg (0.314 mmol) of S_8 in 90 mL of THF was treated with 0.20 mL (0.942 mmol) of $(Me_3Si)_2S$. The reaction mixture was refluxed for 60 h, resulting in a red solution with a yellow precipitate. The yellow precipitate was collected and then extracted into ~200 mL of H_2O. After filtration of the extract to remove a small amount of brown solid, the filtrate was worked up as above to give 0.096 g of **[2]**$(PF_6)_2$ (18%).

[1]$(PF_6)_2$: FAB MS 1303 (M^+); ^1H NMR (CD_2Cl_2, 38 °C) δ 1.84 (s, $C_5\mathit{Me}_5$). ^1H NMR (CD_2Cl_2, −37 °C) δ 1.91 (s, 30H), 1.66 (s, 30H). $^{13}C\{^1H\}$ NMR (CD_2Cl_2, −37 °C) δ 105.1 (s, C_5Me_5), 94.0 (s, C_5Me_5), 9.63 (s, $C_5\mathit{Me}_5$), 8.38 (s, $C_5\mathit{Me}_5$). ^{13}C CP-MAS δ 105.23, 106.9, 95.7 (C_5Me_5), 9.99, 9.25 ($C_5\mathit{Me}_5$). UV–vis (CH_2Cl_2, λ, log ε) 336 (3.13), 410 (2.64), 636 (1.99). Anal. Calcd for $C_{40}H_{60}F_{12}Ir_4P_2S_4$: C, 27.80; H, 3.49; F, 13.19; Ir, 44.49; P, 3.58; S, 7.42. Found: C, 27.84; H, 3.48; F, 13.12; Ir, 44.55; P, 3.51; S, 7.45.

[2]$(PF_6)_2$: FAB MS 1046 (M^+). ^1H NMR (CD_3CN) δ 2.25 (s, C_5Me_5). ^{13}C NMR (CD_2Cl_2) δ 100.7 (C_5Me_5), 11.35 ($C_5\mathit{Me}_5$). UV–vis (CH_2Cl_2, λ, log ε) 338 (2.04). Anal. Calcd for $C_{30}H_{45}F_{12}Ir_3P_2S_2$: C, 26.96; H, 3.39; Ir, 43.15; P, 4.50; S, 4.80. Found: C, 26.97; H, 3.41; Ir, 43.55; P, 4.50; S, 4.72.

$[(C_5Me_5)_3Ir_3S_2]$, [2]^0. A solution of 0.350 g (0.262 mmol) of $[(C_5Me_5)_3Ir_3S_2](PF_6)_2$ in 20 mL of CH_3CN was transferred via cannula to a solution of 0.099 g (0.5238 mmol) of $(C_5H_5)_2Co$ in 20 mL of CH_3CN. The solution immediately turned brown. After 2 h, the solvent was removed in vacuo. The residue was extracted into 30 mL of benzene and the extract was filtered to remove $(C_5H_5)_2CoPF_6$ and evaporated to dryness. The dry powder was heated in vacuo at 40 °C (1 mmHg) for 4 h to sublime unreacted $(C_5H_5)_2Co$. There remained 0.263 g of an extremely air-sensitive dark blue residue (96%). ^1H NMR ($C_6D_5CD_3$, 100 °C) δ 1.92 (br, s, 3 H). ^1H NMR ($C_6D_5CD_3$, −37 °C) δ 2.29 (s, 1H), 1.90 (s, 2H). ^{13}C NMR ($C_6D_5CD_3$, −37 °C) δ 8.88 (C_5Me_5), 85.2 (C_5Me_5), 11.98 ($C_5\mathit{Me}_5$), 10.92 ($C_5\mathit{Me}_5$). UV–vis (CH_3CN, λ, log ε) 592 (2.28). Anal. Calcd for $C_{30}H_{45}Ir_3S_2$: C, 34.44; H, 4.33; S, 6.12. Found: C, 34.97; H, 4.35; S, 6.02.

Preparation of [1](PF$_6$)$_2$ for DNMR Measurements. Due to difficulty in removing trace solvent impurities from the samples prepared as above, the DNMR sample was prepared as follows: A solution of 0.221 g (0.213 mmol) of $(C_5Me_5)_4Ir_4S_4$ in 10 mL of CH_2Cl_2 was treated with 0.141 g (0.426 mmol) of $(C_5H_5)_2FePF_6$ in 60 mL of CH_2Cl_2, resulting in a green solution. After 1.5 h the solution was concentrated to 10 mL and diluted with 60 mL of benzene to give 0.331 g of $[(C_5Me_5)_4Ir_4S_4](PF_6)_2$ (90% yield).

Crystallography of [1](PF$_6$)$_2$. Crystals of **[1]**$(PF_6)_2$ were grown by diffusion of hexanes into an acetone solution of the cluster. Data were collected on an opaque green-brown plate of dimensions 0.06 × 0.2 × 0.3 mm mounted on a glass fiber. **[1]**$(PF_6)_2$ crystallizes in the triclinic space group $P\bar{1}$ with a = 11.447(4) Å, b = 12.265(6) Å, c = 20.470(14) Å, α = 91.48(5)°, β = 95.99(4)°, γ = 91.47(4)°, Z = 2, and d_{calcd} = 2.009 g/cm^3. 8374 unique reflections were refined to a final R = 0.0595 and R_w = 0.0673. The positions of the iridium and sulfur atoms were obtained by direct methods. The remaining atoms were located by cycles of least-squares refinement and difference Fourier maps using the SHELXS-76 programs (G. Sheldrick, Nicolet XRD, Madison, WI).[34] Both PF_6^- anions were disordered in at least two positions, therefore octahedral geometry was imposed on each disordered group and refined between two fractional occupations. Isotropic parameters were refined for F and C atoms, with common P–F and C–C bond lengths refined. The Ir and S atoms were independently refined with anisotropic thermal coefficients. The highest peak in the difference Fourier map corresponding to 2 e$^-$ was 0.95 Å from Ir(2). Selected bond distances and angles are listed in Table 3. Calculations of H···H contacts were made with Cambridge Scientific's Chem 3-D program assuming C–H distances of 0.08 Å and C–C–H angles of 109°.

Crystallography of [2](PF$_6$)$_2$. Crystals of **[2]**$(PF_6)_2$ were grown by diffusion of hexanes into an acetone solution of the cluster. An orange crystal of dimensions 0.2 × 0.3 × 0.3 mm was mounted on a glass fiber. **[2]**$(PF_6)_2$ crystallizes in the monoclinic space group $P2_1/c$ with a = 13.066(3) Å, b = 20.088(6) Å, c = 16.262(4) Å, α = γ = 90, β = 98.54°, Z = 4, and d_{calcd} = 2.103 g/cm^3. Of 7088 reflections collected, 6853 unique data were refined to a final R = 0.0445 and R_w = 0.0465. The iridium and sulfur positions were deduced by direct methods. The remaining atoms were located by cycles of least-squares refinement and differences Fourier maps using the SHELXS-76 programs.[23] Hydrogen atoms were introduced at calculated positions, used for structure factor calculations, and refined with common isotropic thermal parameters. Both PF_6^- anions were disordered in at least two positions, therefore octahedral geometry was imposed and the constrained groups were refined in two orientations each. Isotropic parameters were refined for F and C atoms, and a common P–F bond length was refined. The remaining atoms were refined anisotropically. The highest peak in the difference Fourier map corresponded to 2 e$^-$ in the vicinity of the disordered anions. Selected bond distances and angles are listed in Table 4.

Acknowledgment. This research was supported by the National Science Foundation. Johnson Matthey is thanked for the loan of iridium trichloride.

Supplementary Material Available: Tables of atomic coordinates, bond lengths and angles, and anisotropic thermal parameters (25 pages); tables of observed and calculated structure factors (73 pages). This material is contained in many libraries on microfiche, immediately follows this article in the microfilm version of the journal, and can be ordered from the ACS; see any current masthead page for ordering information.

(34) (a) Stout, G. H.; Jensen, L. H. *X-Ray Structure Determination, a Practical Guide*; Macmillan: New York, 1968. (b) Sheldrick, G. M. SHELXS-76, a program for crystal structure determination, University Chemical Laboratory, Cambridge, England, 1976.